Changing tidal hydrodynamics during different stages of eco-geomorphological development of a tidal marsh : a numerical modeling study

Stark, J., Meire, P., Temmerman, S. (2017). Changing tidal hydrodynamics during different stages of eco-geomorphological development of a tidal marsh: A numerical modeling study. Estuarine, Coastal and Shelf Science, 188: 56-68. doi: 10.1016/j.ecss.2017.02.014

Corresponding author:

Jeroen Stark
University of Antwerp - Ecosystem Management Research Group
Universiteitsplein 1 C1.10 | BE-2610 Antwerpen
jeroen.stark@uantwerpen.be / jeroenstark@hotmail.com

Keywords:

- hydrodynamic modelling
- tidal propagation
- marsh
- geomorphology
- The Netherlands

Abstract

The eco-geomorphological development of tidal marshes, from initially low-elevated bare tidal flats up to a high-elevated marsh and its typical network of channels and creeks, induces long-term changes in tidal hydrodynamics in a marsh, which will have feedback effects on the marsh development. We use a two-dimensional hydrodynamic model of the Saeftinghe marsh (Netherlands) to study tidal hydrodynamics, and tidal asymmetry in particular, for model scenarios with different input bathymetries and vegetation coverages that represent different stages of eco-geomorphological marsh development, from a low elevation stage with low vegetation coverage to a high and fully vegetated marsh platform. Tidal asymmetry is quantified along a 4 km marsh channel by (1) the difference in peak flood and peak ebb velocities, (2) the ratio between duration of the rising tide and the falling tide and (3) the time-integrated dimensionless bed shear stress during flood and ebb. Although spatial variations in tidal asymmetry are large and the different indicators for tidal asymmetry do not always respond similarly to eco-geomorphological changes, some general trends can be obtained. Flood-dominance prevails during the initial bare stage of a low-lying tidal flat. Vegetation establishment and platform expansion lead to marsh-scale flow concentration to the bare channels, causing an increase in tidal prism in the channels along with a less flood-dominant asymmetry of the horizontal tide. The decrease in flood-dominance continues as the platform grows vertically and the sediment-demand of the platform decreases. However, when the platform elevation gets sufficiently high in the tidal frame and part of the spring-neap cycle is confined to the channels, the discharge in the channels decreases and tidal asymmetry becomes more flood-dominant again, indicating an infilling of the marsh channels. Furthermore, model results suggest that hydro-morphodynamic feedbacks based on tidal prism to channel cross-sectional area relationships keep the marsh channels from filling in completely by enhancing ebb-dominance as long as the tidal volume and flow velocities remain sufficiently high. Overall, this study increases insight into the hydro-morphodynamic interactions between tidal flow and marsh geomorphology during various stages of eco-geomorphological development of marshes and marsh channels in particular.

1. Introduction

Tidal marshes along estuaries and coasts form a unique habitat and are highly valuable (Barbier et al., 2013). Their ecological functioning provides benefits to society such as improvement of water quality (e.g., Mitsch et al., 2012), carbon sequestration (e.g., McLeod, 2011; Mitsch et al., 2013; Ouyang and Lee, 2014) or flood and shoreline erosion protection (e.g., Stark et al., 2016; Gedan et al., 2010; Spalding et al., 2014; Temmerman and Kirwan, 2015; Temmerman et al., 2013). The sustainability of tidal marshes and their functions is however under pressure by among others sea level rise and anthropogenic impacts (Kirwan and Megonigal, 2013; Kirwan et al., 2016). A key aspect for the functioning and sustainability of tidal marshes are the fluxes of water and the physical, chemical and biological materials it contains (i.e., sediments, nutrients, pollutants, seeds, larvae, plankton, etc.) through tidal channels that connect marshes with the adjacent estuary or sea. For example, denitrification (e.g. Mitsch et al., 2012) or biogenic silica recycling (e.g. Struyf et al., 2005) depend on the water exchange between marshes and adjacent seas or estuaries and are therefore closely related to the tidal prism (Fagherazzi et al., 2013). Other ecological functions such as carbon and nitrogen burial are related to sediment deposition in marshes (McLeod et al., 2011; Mitsch et al., 2012) and hence to the sediment transport through marsh channels. The tidal asymmetry in the channels, which describes the difference in magnitude and duration of flood and ebb fluxes, determines whether marsh systems are a net sink (import) or source (export) of these materials (e.g. Fagherazzi et al., 2013; French and Stoddart, 1992; Friedrichs and Perry, 2001). Moreover, a flood or ebb dominant asymmetry respectively generates net sediment import or export and ultimately determines the marshes' ability to build up sediments and hence to sustain themselves in balance with sea level rise (e.g. Ganju et al., 2015, 2013; Reed, 2002).

In general it is well-known that the tidal wave is distorted and may become asymmetric as it propagates through shallow channels due to processes including bottom friction, channel convergence and advective inertia (e.g. Aubrey and Speer, 1985; Friedrichs and Aubrey, 1988; Parker, 1984; Speer and Aubrey, 1985; Wang et al., 1999). A distinction can be made between the asymmetry of the vertical tide (i.e., water levels) and of the horizontal tide (i.e., discharges and velocities). Vertical tidal asymmetry is here quantified by the difference in duration of the flood and ebb periods. The vertical tide is considered flood dominant if the duration of the flood period is shorter than the duration of the ebb and ebb-dominant if the ebb is shorter than the flood. Horizontal tidal asymmetry is expressed by the difference between

peak currents or discharges during flood and ebb. The horizontal tide is considered flood dominant in case when the peak flood velocities are higher than the peak ebb velocities, and vice versa. The difference in duration of the slack waters (i.e. periods with negligible flow velocities) after high and low tide is another indicator for horizontal tidal asymmetry, as it relates to the deposition of fine sediments after flood and ebb (Dronkers, 1986). However, intertidal marsh channels fall dry at low tide and experience long periods of low water slack without any physical meaning for sediment transport. Therefore, this characterization of tidal asymmetry is deemed not applicable in intertidal channels.

For tidal marshes specifically, numerous field studies have quantified the tidal asymmetry and associated net import or export of materials through marsh channels (e.g. Boon, 1975; French and Stoddart, 1992; Ganju et al., 2015, 2013; Green and Hancock, 2012; Pethick, 1980). However, the factors determining the direction and magnitude of tidal asymmetry in marsh channels are still poorly understood. We hypothesize that one such factor may be the stage of eco-geomorphological development of the combined channel-marsh system. The development of a channel network on an originally bare intertidal flat is most likely initiated by small topographic depressions, which lead to a concentration of tidal flow and thereby locally to higher shear stresses and eventually to creek formation (D'Alpaos et al., 2005; Stefanon et al., 2010). Further development towards a marsh system with a channel network and a vegetated platform is strongly influenced by the establishment of patches of pioneer vegetation. Vegetation patches reduce flow velocities locally and enhance sedimentation inside the patches (Christiansen et al., 2000; De Lima et al., 2015; Mudd et al., 2010), while the flow is accelerated and shear stresses are higher leading to erosion adjacent to the patches (Bouma et al., 2013; D'Alpaos et al., 2006; Temmerman et al., 2007; Vandenbruwaene et al., 2013; Zong and Nepf, 2010). This positive feedback mechanism causes vegetation patches to expand due to increased sedimentation wherever vegetation is present and marsh channels to grow due to increased erosion in between vegetation patches, eventually leading to merging of vegetation patches and the formation of the typical marsh landscape consisting of elevated vegetated platforms dissected by a non-vegetated channel network (Allen, 2000; D'Alpaos et al., 2007; Kirwan and Murray, 2007; Stefanon et al., 2010; Temmerman et al., 2012; Vandenbruwaene et al., 2013). Over the course of a few decades, sedimentation on the vegetated areas raises the elevation of the marsh platform up until around mean high water level (MHWL) (Allen, 2000; Temmerman et al., 2003), depending on external factors including sediment supply and rate of sea level rise (e.g., French, 2006; Kirwan et al., 2010; Temmerman et al., 2004). It may be

expected that the establishment of marsh vegetation and the elevation increase of the vegetated platform induce contradicting effects on the flow pattern through the marsh channels. The friction caused by the vegetation and the vertical growth of the marsh platform are expected to enhance flow concentration towards the channels and thereby increase the tidal discharge in the channels. However, less water can be stored on higher platforms, leading to a smaller tidal prism and lower tidal discharge through the channels (D'Alpaos et al., 2006; Temmerman et al., 2007). Along with these effects of marsh developmental stage on tidal discharges in the channels, we may expect that the degree of tidal asymmetry, and hence the net material fluxes, will change during different stages of marsh and channel development, but this has not been systematically documented.

Here, we assess tidal hydrodynamics in marsh channels during different stages of marsh development, starting from a low-lying, almost bare tidal flat situation up to a high-elevated, vegetated marsh with a platform elevation around mean high water level. The selection of these marsh developmental stages is based on observations over a long time scale (ca. 80 years) in a large marsh (ca. 3000 ha) in the Netherlands (Wang and Temmerman, 2013). A validated two-dimensional hydrodynamic model for this channel-marsh system (Stark et al., 2016) is used to assess vertical and horizontal tidal asymmetry for a number of observed successive stages of marsh development. Finally, we discuss the implications of our model results in terms of expected effects on net material flux and how this evolves during different stages of marsh development.

2. Methods

2.1 Study Area

We study tidal hydrodynamics in the intertidal channels of the 'Verdronken Land van Saeftinghe' (in the following: 'Saeftinghe'), a ca. 3000 ha tidal marsh along the Western Scheldt (Figure 1). The present-day marsh is surrounded by levees in the south and the west and bordered by the subtidal estuary channel in the north and east. Three large intertidal channels characterize the marsh geomorphology throughout its development since 1900. (Figure 2a-c). The most eastward channel (*'Hondegat'*) and adjacent marshes are the subject of this study. Detailed field measurements of tidal water level movements (Stark et al., 2015) and a validated two-dimensional hydrodynamic model (Stark et al., 2016) are available for this area. The marsh platform is covered by various types of vegetation, of which *Elymus athericus* and *Scirpus maritimus* are the most abundant (Vandenbruwaene et al., 2015). Nowadays, a semi-diurnal macrotidal regime induces a tidal range of 4.0-5.6 m in the estuary channel adjacent to the study area. High water levels at the study area vary between 2.18 m and 3.15 m above NAP (NAP is the Dutch ordnance level, close to mean sea level), with a MHWL of 2.76 m.

Wang and Temmerman (2013) presented an analysis of the eco-geomorphological development of the Saeftinghe marsh from the 1930s until 2004 using historical digital elevation models (DEMs) and vegetation maps. These maps are based on topographic surveys and aerial photographs provided by Rijkswaterstaat (Huijs, 1995; Tolman and Pranger, 2012). Here, we extend this analysis until 2010-2013. In particular, the vegetation cover and geomorphology of Saeftinghe is visualized in Figure 2a-c and summarized in Table 1 for the 1930s (1931 DEM and 1935 vegetation map), 1960s (1963 DEM and 1959 vegetation map) and 2010s (2013 DEM and 2010 vegetation map). Furthermore, the elevation changes are depicted as well in Figure 2e-f. Marsh expansion occurred mostly towards the northern part of Saeftinghe, but also locally at the marsh-channel edges. The most southern and eastern parts of Saeftinghe, close to the levees, had already developed to a relatively high vegetated marsh state in the 1930s. The remaining part of the marsh developed from a low and mostly unvegetated tidal flat to a high and vegetated marsh and channel system during the studied period.

Table 1. Development of the elevation and vegetation cover of the Saeftinghe marsh and of the mean high water level (MHWL) in the adjacent estuary channel.

Period	***1931-1935***	***1959-1963***	***2010-2013***
Mean elevation	1.13 m NAP	2.18 m NAP	2.41 m NAP
Mean elevation bare flats	0.56 m NAP	0.99 m NAP	1.05 m NAP
Mean elevation vegetated platform	1.92 m NAP	2.69 m NAP	2.99 m NAP
Vegetation cover	48%	67%	69%
MHWL	2.36 m NAP	2.53 m NAP	2.76 m NAP

2.2 Hydrodynamic model

2.2.1 Model description

A previously calibrated and validated Telemac-2D model of the Scheldt Estuary is adopted from earlier studies (Smolders et al., 2015, 2012; Stark et al., 2016) and used in the present study to perform hydrodynamic model scenarios that cover different stages of marsh and channel development (i.e., using different input bathymetries and vegetation coverages). Telemac-2D is a widely used modeling system that is part of the Telemac-Mascaret modeling suite. It solves the Saint-Venant equations in two dimensions and contains the relevant physical processes with respect to tidal wave propagation in estuaries (Hervouet, 2007). Wetting and drying is treated numerically in a mass-conservative way by allowing slightly negative depths and smoothing water level gradients when nodes in the model domain fall dry. The present model comprises the Scheldt Estuary from the North Sea up to its upstream tributaries (Figure 1). Mesh sizes range from approximately 10-50 m in the upstream tributaries up to about 150-200 m in the downstream part of the estuary. The mesh is refined at the marsh study area to a mesh size of ~6-20 m in order to include the marsh geomorphology and its channel system as good as possible. More specifically, the width of the studied marsh channel is represented by 5 or more elements. An even further refinement of the mesh would lead to undesirably long computation times. Historical elevation data of the marsh (Figure 2a-c) is interpolated to a 20 x 20 m DEM and used to implement the marsh morphology. To compute bottom friction, Telemac-2D uses a dimensionless coefficient, c_f, defined as: $2 \cdot g \cdot n^2/(h^{1/3})$, in which g is the gravitational acceleration ($m \cdot s^{-2}$), n is a predefined Manning friction coefficient ($s \cdot m^{-1/3}$) and h is the water depth (m). Vegetation effects on tidal flow over the marsh platform are simply implemented by increasing bottom friction coefficients wherever vegetation is present. This means that depth-dependent effects of the

vegetation (i.e., submerged versus emerged) on the flow are thus not incorporated (Baptist et al., 2007). For additional information on Telemac-2D we refer to (Hervouet, 2007) and the user manual (see: http://wiki.opentelemac.org/).

The North Sea boundary is forced with 28 days (i.e., 1/7/2012-28/7/2012) of water level observations from tide gauges in the coastal zone. Upstream discharges are not implemented as the influence of the upstream freshwater discharge on tidal hydrodynamics in the studied marsh can be considered negligible. In particular, the total discharge of the upstream tributaries ranged between 50 and 174 m^3/s during the simulation period (Vanlierde et al., 2013), which is less than one percent of the amplitude of the tide-induced discharges through the estuarine channel adjacent to the Saeftinghe marsh.

2.2.2 Model calibration

Calibration of the Saeftinghe model was done previously based on the 2011 bathymetry by varying Manning's bottom friction coefficients for the non-vegetated intertidal channels (n_f) between 0.01 to 0.03 $s \cdot m^{-1/3}$ and for the vegetated marsh platform (n_v) between 0.04 and 0.12 $s \cdot m^{-1/3}$; and by varying the spatially and temporally constant velocity diffusivity coefficient (ν) between 0.01 and 10 $m^2 \cdot s^{-1}$ (see: Stark et al., 2016). Ultimately, calibration on the representation of (high) water levels in the marsh channels resulted in the following settings: ν = 0.5 $m^2 \cdot s^{-1}$, n_f = 0.01 $s \cdot m^{-1/3}$ and n_v = 0.08 $s \cdot m^{-1/3}$. It should be stated that ν is related to (local) mesh size and was optimized for the studied marsh where the mesh is refined. Therefore, its value might not be optimal for other areas in the model (outside of the marsh study area that is the focus of the present paper) with a much finer or coarser mesh. Besides, care was taken throughout the calibration process that changes in model settings did not affect the performance of the previously validated estuary scale model.

2.2.3 Model validation

The model performance on estuary scale was previously assessed based on observed water levels and stage-discharge curves (Smolders et al., 2015, 2012). Similarly, the model was previously validated on marsh scale with observed water level data along the studied marsh channel (Stark et al., 2016). Validation showed that observed water levels in the marsh channels are represented with mean errors between -0.02 m and -0.11 m, indicating that the water levels are slightly underestimated in the marsh system. Furthermore, peak water levels are represented with mean errors between -0.03 m and +0.05 m (or ~1% of the local tidal range), which is a similar accuracy as in the adjacent estuarine channels.

Here, we extend the model validation by comparing modelled flow velocities with velocity measurements conducted in 2012 (provided by Rijkswaterstaat Zeeland – Meetadviesdienst) at locations a, b, c and d in the studied marsh channel (see Figure 2d). Mean errors (ME) root mean squared errors (RMSE) and normalized root mean squared errors (NRMSE; i.e., RMSE normalized by the range of the total dataset) are calculated for the full series of flow velocities (Table 2). Validation is also done for peak velocities specifically (Table 2; Figure 3). The model represents the full series of observed flow velocities with a relative ME at locations b and c, where velocities are highest, of -18% and -1% respectively. At locations a and d, velocities are underestimated by approximately -30% on average. Values for RMSE are all around ~0.08 m/s, which is 15-17% of the range of the observations depending on the location. Peak flood currents and to a lesser extent peak ebb currents are generally overestimated (Figure 3), except for the peak ebb velocities at location a where the peak ebb velocities are underestimated (Table 2). RMSE values for peak flood velocities are between 0.06-0.19 m/s (i.e., 25-36% of the range in observed peak velocities) and between 0.06-0.13 m/s (i.e., 17-24% of the range in peak ebb velocities) for peak ebb velocities. The model generally overestimates peak flood velocities more than peak ebb velocities, which will affect the modelled horizontal tidal asymmetry. In particular, the difference between peak flood and peak ebb velocities is on average overestimated by 0.19 m/s, 0.21 m/s, 0.11 m/s and 0.09 m/s for locations a, b, c and d respectively. Therefore, the results on tidal asymmetry in this study should be interpreted with care.

Table 2. Validation of the model with observed flow velocities at locations shown in Figure 2d, depicting the mean error, root mean squared error and normalized root mean squared error of the full series of flow velocities and for the flood and ebb peak flow velocities.

Measurement	**Total series**			**Flood peak**			**Ebb peak**		
location	**ME**	**RMSE**	**NRMSE**	**ME**	**RMSE**	**NRMSE**	**ME**	**RMSE**	**NRMSE**
	m/s	*m/s*	-	*m/s*	*m/s*	-	*m/s*	*m/s*	-
a	-0.08	0.07	0.17	+0.01	0.06	0.25	-0.05	0.08	0.18
b	-0.04	0.08	0.15	+0.16	0.17	0.36	+0.06	0.10	0.17
c	0.00	0.08	0.15	+0.18	0.19	0.32	+0.10	0.13	0.21
d	+0.05	0.08	0.16	+0.11	0.16	0.30	+0.05	0.06	0.24

2.3 Model scenarios

Several model scenarios are set up to analyze the effect of successive development stages of marsh geomorphology (based on historical DEMs) and vegetation cover (based on vegetation

maps) on tidal asymmetry in an intertidal marsh channel (Table 3). Scenario sc1 represents the mudflat stage as the effects of vegetation are left out and the elevation of the marsh platform was still rather low in the 1930s. Scenarios sc2, sc5 and sc6 contain the historical development from a relatively low marsh in the 1930s (sc2) to the 1960s (sc5) and finally a high marsh in the 2010s scenario (sc6). Scenarios sc3 and sc4 consider a stepwise development of vegetation expansion (sc2 to sc3) and platform elevation increase (sc3 to sc4) between the 1930s scenario and 1960s scenario. Finally, scenarios sc7 and sc8 investigate the effect of continuous infilling of the marsh channels. The channel elevation increase in these scenarios is limited to a maximum elevation of 2.5 m above NAP to avoid that the channels become higher than the surrounding marsh platform, resulting in an average channel elevation increase of 0.4 m in sc7 and 0.7 m in sc8.

Table 3. Overview of the model scenarios.

Scenario	**Geomorphology**	**Vegetation cover**	**Marsh development steps / stage**
sc1	1931	None	*'low and bare tidal flat'*
sc2	1931	1935	*vegetation establishment*
sc3	1931	1959	*vegetation establishment*
sc4	1931 channels / 1963 platform	1959	*vertical platform growth*
sc5	1963	1959	*channel infilling*
sc6	2013	2010	*vertical platform growth & channel infilling*
sc7	2013 (channels + 0.4 m)	2010	*continued channel infilling*
sc8	2013 (channels + 0.7 m)	2010	*continued channel infilling*

Only the topography and vegetation cover of the marsh itself vary between the different scenarios, while the bathymetry in the rest of the model is kept constant to exclude effects of external changes (i.e., morphological development in the rest of the Scheldt estuary). The hydrodynamic boundary conditions are kept constant as well. This implies however that the MHWLs at the studied marsh are higher in some model scenarios than the historical MHWLs in the 1930s and 1960s (i.e., 2.36 m in 1930, 2.53 m in 1960 and 2.76 m in 2010), implying that the marsh has a lower position in the tidal frame. Hence, the model scenarios do not represent the historical situation as such, but allow for an analysis of changing tidal hydrodynamics as a result of the geomorphological development of a tidal marsh without having to account for long term variations in external factors such as changes in tidal range, MHWL or sea level rise. The impact of changing MHWLs on the model results is assessed by two additional model runs in which scenarios sc2 (1930s) and sc5 (1960s) are simulated with

adjusted boundary conditions. In these model runs, the tidal amplitude at the boundary is reduced such that the simulated MHWL near the study area is similar to the MHWL of the 1930s for sc2 and of the 1960s for sc5.

2.4 Analysis of marsh geomorphology and tidal asymmetry

We analyze the simulated variation in tidal asymmetry throughout different stages of marsh development more specifically at three cross-sections along the Hondegat channel (sections H1-H3 in Figure 2d). The geomorphological development of the marsh channel is assessed locally by calculating the mean and minimum channel elevation (i.e., corresponding to the mean and maximum water depth in the channel), channel width and channel cross-sectional area. Intertidal flats above +2.0 m NAP (~0.7 m below MHWL) are not considered part of the channel network anymore as a shift between bare and vegetated states is present around this elevation in the studied marsh (Wang and Temmerman, 2013). The vegetation cover in the proximity of the channel sections is calculated for a 500 m wide buffer zone around the sections. Finally, the geomorphological development of the marsh platform surrounding the Hondegat channel is qualitatively assessed based on the elevation changes in Figure 1.

Tidal asymmetry is quantified here in two ways: (1) as the average ratio between the duration of rising and falling tide, R_T, and (2) as the average difference between flood and ebb peak velocities (ΔV_{max}):

$$R_T = \frac{1}{n}\sum_{j=1}^{n}\left(\frac{T_{rise}(j)}{T_{fall}(j)}\right) \quad \text{(Eq.1)}$$

$$\Delta V_{max} = \frac{1}{n}\sum_{j=1}^{n}(V_{max}flood(j) - V_{max}ebb(j)) \quad \text{(Eq.2)}$$

in which T_{rise} and T_{fall} are the durations (in min) of water level rise and water level fall for each tide, $V_{max\text{-}flood}$ and $V_{max\text{-}ebb}$ represent the maximum cross-sectional averaged flood and ebb velocities per tide (in m/s), j represents an individual tide and n is the amount of tides in the simulation. For the calculation of R_T, the long period of gravity-induced ebb drainage with relatively slow flow velocities, low water depths and hence little physical meaning for sediment transport is excluded from the calculation by limiting T_{fall} to the period during which the water level fall is higher than 0.4 cm/min. This limit corresponds with a shift in the rate of water level change, visible in the model results, from faster tidally induced outflow to slower gravity-induced outflow due to friction-induced lagging effects on the ebb. Besides, as the

sediment in the main channels of the Saeftinghe mainly consists of fine sand (Jongepier et al., 2015), the difference between maximum flood and ebb velocities can be considered as an indicator for the residual sediment transport load and direction (Van de Kreeke and Robaczewska, 1993; Wang et al., 1999).

An additional indicator for tidal asymmetry considered here is the (dimensionless) bed shear stress relative to the critical bed shear stress for the initiation of particle motion. This parameter is often used in sediment transport formulas (e.g. Chollet and Cunge, 1979) and may be used as a proxy for the sediment transport and hence as an indicator for horizontal tidal asymmetry. We emphasize that it is not our intention to use this proxy as an estimate of actual sediment transport, but for this study, it provides insight in the variations in horizontal tidal asymmetry, while considering the entire tidal wave (i.e., the full velocity time series) instead of solely peak velocities. Total sediment transport correlates with the excess dimensionless bed shear stress to the power ~1.5 (e.g. Van Rijn, 1993):

$$Q_s \sim \frac{1}{t}\sum_{i=1}^{t}(\theta(i)-\theta_{cr})^{1.5} \quad \text{for} \quad \theta(i) > \theta_{cr} \qquad \text{(Eq.3)}$$

in which Q_s represents the cumulated excess bed shear stress over the entire simulation of t time steps, $\theta(i)$ is the time-varying non-dimensional bed shear stress and θ_{cr} is the critical non-dimensional shear stress for the initiation of particle motion. We distinguish between flood and ebb flow by assigning positive values to the results during flood and negative values during ebb. By doing so, we obtain a residual value for $(\theta-\theta_{cr})^{1.5}$ over a full spring-neap cycle which can be flood- or ebb-dominant. The dimensionless bed shear stress θ is calculated as follows:

$$\theta(i) = \frac{1}{d_{50}\cdot(s-1)}\cdot\left(\frac{V(i)}{C(i)}\right)^2 \qquad \text{(Eq.4)}$$

in which $V(i)$ represents the flow velocity per time step (m/s), extracted from the model results at every 5 m along cross-sections H1, H2 and H3. Furthermore, s is the relative density of the sediment (-) and d_{50} is the median grain size (m). The Chézy friction coefficient $C(i)$ ($m^{1/2}/s$) depends on the time-varying water depth based on:

$$C(i) = 5.75\cdot\sqrt{g}\cdot\log\left(\frac{12h(i)}{6d_{50}}\right) \qquad \text{(Eq.5)}$$

with *h(i)* being the time-varying water depth (m), which is also extracted from the hydrodynamic model results, and g the gravitational acceleration (m/s^2). The critical dimensionless shear stress θ_{cr} is a function of the dimensionless particle parameter D_* (Van Rijn, 2007a) and can be estimated by:

$$\theta_{cr} = 0.115 \cdot (D_*)^{-0.5} \qquad \text{for } D_* < 4 \qquad \text{(Eq.6a)}$$

$$\theta_{cr} = 0.14 \cdot (D_*)^{-0.64} \qquad \text{if } 4 \leq D_* < 10 \qquad \text{(Eq.6b)}$$

with: $$D_* = d_{50} \cdot \left(\frac{(s-1) \cdot g}{{\upsilon_k}^2}\right)^{1/3} \qquad \text{(Eq.6c)}$$

in which υ_k is a kinematic viscosity coefficient (m^2/s). For the calculations, the parameters are set as follows: s = 2.65, d_{50} = 150 μm (the main channels of Saeftinghe typically consist of fine sand with a d_{50} of 125 to 250 μm; Jongepier et al., 2015; Ysebaert and Herman, 2002), g = 9.81 m/s^2, υ_k = 10^{-6} m^2/s (Van Rijn, 2007b), while *C(i)* mostly ranges between 55 and 75 m$^{1/2}$/s depending on the water depth. These settings result in D_* = 3.8 and a critical dimensionless shear stress for the initiation of particle motion of θ_{cr} = 0.0595. The latter implies that the velocity threshold for particle motion varies from 0.21 m/s to 0.29 m/s along with the depth-dependent Chézy coefficient. Ultimately, the results are cumulated per cross-section (i.e., H1, H2 and H3). The above approach is for non-cohesive sediments, whereas in reality cohesive sediments, for which the mobility criterion and the relation between excess bed shear stress and sediment transport are different (e.g. Van Rijn, 2007a, 1993), are present as well (i.e., especially in the smaller channel sections; Hampel et al., 2003). Therefore, we want to emphasize that this proxy for residual sediment transport should solely be interpreted as an indicator for horizontal tidal asymmetry and has little predictive value for the actual sediment transport.

Finally, we compute the average spring tidal prism (*P*) and compare it with a typical power law relationship between channel cross-sectional area (*Ω*) and tidal prism. Such general relationships have been found for tidal inlet channels (e.g. D'Alpaos et al., 2009; Jarrett, 1976; O'Brien, 1969, 1931; Stive et al., 2010), but also for marsh channels specifically (e.g. Rinaldo et al., 1999; Steel and Pye, 1997; Vandenbruwaene et al., 2015). Here, a Ω-to-P relationship is obtained by making a power law fit through the simulated tidal prisms and the cross-sectional areas at multiple cross-sections along the Hondegat channel for the present-day scenario (i.e., sc6).

3. Results

3.1 Geomorphological development

The eco-geomorphological development of the marsh is quantified by the changes in vegetation cover and channel geometry at sections H1, H2 and H3 (see Figures 1d) along the studied marsh channel (Figure 4). Vegetation cover increased the strongest in the outer part of the marsh near location H1, whereas it was already high in the 1930s at the more inland locations H2 and H3 (Figure 4a). From the 1960s onwards (i.e., sc5 to sc8), the vegetation cover remained nearly constant around all three sections. The platform elevation along the marsh channel increases strongly between the 1930s scenario to the 1960s scenario (i.e., sc3 to sc4) and less pronounced between the 1960s and 2010s scenarios (i.e., sc4/5 to sc6) (Figure 1e/f). The cross-sectional area of the channels generally decreases between the consecutive model scenarios at all three locations (i.e., sc3 to sc8), except for the channel size increase at H1 between the 1960s (sc5) and 2010s (sc6). Besides, this local increase in channel size at section H1 is likely due to the development of a connecting channel between the Hondegat channel and the middle main channel of the Saeftinghe marsh, which established in the 2010s scenario (Figure 1) and enlarges the watershed and hence tidal prism of the Hondegat channel at section H1. Sections H2 and H3 sections are not affected as these are located 'upstream' of this side-branch. The decreasing cross-sectional area is mainly due to an increasing elevation of the channel bed for scenarios sc4 to sc5 and sc6 to sc8 at H1, sc5 to sc8 at H2 and sc5 to sc8 at H3. However, for scenarios sc7 to sc8 at section H1 and sc6 to sc8 at sections H2 and H3, the elevation increase of the marsh channel bed is also accompanied by a reduction in channel width. Deepening of the channel is present as well between scenarios sc3 to sc4 and sc5 to sc6 at H1 and sc3 to sc5 at H3, implying that the decrease in cross-sectional area between sc3 and sc4 at section H1 and between sc3 and sc5 at section H3 is solely the result of channel narrowing.

In the following, the results of the model scenarios are grouped based on specific eco-geomorphological developments of the marsh: vegetation establishment (sc1, sc2 and sc3); vertical platform growth (sc3, sc4 and sc6); channel size increase (sc5 to sc6 at section H1); and channel size decrease (sc4 to sc5 and sc7 to sc8 at H1 and sc4 to sc8 at H2 and H3).

3.2 Tidal Prism

The tidal prism in the studied marsh channel generally decreases between the consecutive scenarios (Figure 5a) as a result of overall marsh elevation increase (Table 1 and Figure 1)

and consequently decreasing storage volume. In Figure 5b, the simulated tidal prism is plotted against the cross-sectional areas of each channel section for all scenarios and compared with a cross-sectional area to prism relationship for the marsh channel based on the simulation results of the present-day scenario (sc6):

$$\Omega = 0.0124 \cdot P^{0.79} \quad \text{(Eq.7)}$$

in which Ω is the cross-sectional area in m² of the marsh channel below MHWL (i.e., below 2.76 m NAP) and P is the mean tidal prism in m³ over the 28-days simulation. Adding the effect of vegetation generally increases the tidal prism in the marsh channels, which causes P to become relatively large for the cross-section based on the above Ω-to-P relationship. Vertical platform growth towards the 1960s level (i.e., sc3 to sc4) leads to a significant decrease in tidal prism and sets P closer to equilibrium with the cross-sectional area of the channels based on the estimated Ω-to-P relationship. At section H2, the tidal prism decreases further for the 2010s scenario (sc6). Conversely, at section H1 the increase in channel size towards the 2010s scenario (i.e., sc5 to sc6) causes the tidal prism to increase despite the vertical platform growth between those scenarios. In both cases, the tidal prism changes in accordance with the estimated Ω-to-P relationship. In scenarios sc7 and sc8, the tidal prism decreases along with the channel size.

3.3 Asymmetry of the vertical tide

The asymmetry of the vertical tide, quantified by the ratio R_T between the duration of the rising tide and the duration of the falling tide (Figure 6a), is consistently shorter-rising along the marsh channel for all eco-geomorphological scenarios. Including the effect of vegetation generally reduces R_T along the marsh channel, except for the small increase in R_T between sc1 and sc2 at locations H1 and H2. Model results indicate that adding the effect of vegetation mainly induces a lagging effect on the falling tide, whereas the duration of the rising tide remains fairly constant. Vertical platform growth (i.e., sc3 to sc4) generally leads to an increase in R_T and hence a development towards a less flood-dominant asymmetry of the vertical tide. The reduction in channel cross-sectional area that is present between various scenarios has varying effects on R_T. At the outer section H1, R_T increases at first between sc4 and sc5, but R_T decreases in the scenarios in which the channel elevation is artificially increased (i.e., sc7 and sc8). Conversely, R_T decreases at the inner marsh sections H2 and H3 between scenarios sc4 and sc6, whereas R_T increases in the following scenarios sc7 and sc8

where the shortening of the falling tide is more profound than the shortening of the rising tide. Finally, the channel size increase from sc5 to sc6 at section H1 slightly enhances R_T.

With respect to the implications of R_T for the horizontal tidal asymmetry, it must be stated that the cumulated flood and ebb volumes are not equal for all examined sections and scenarios. This may affect the link between vertical and horizontal tidal asymmetry. In particular, sc1 gives cumulated flood volumes that are 1.26 times higher than the cumulated ebb volume at loc. H1. Moreover, the flood tidal prism is 0.86 to 0.94 times smaller than the ebb tidal prism for sc2-5 at location H3. For the other scenarios, the cumulated ebb- and flood discharges are nearly equal at all three sections.

3.4 Asymmetry of the horizontal tide

Horizontal tidal asymmetry varies both spatially as well as between the model scenarios (Figure 6b-c & 7). Distinct spatial differences in ΔV_{max} are present along the channel (Figure 7), especially in the proximity of section H2 for sc5, with some channel parts showing a strong flood-dominance, whereas nearby channel parts are strongly ebb-dominant. Such sharp differences are probably caused by local channel morphology. For example, narrow or shallow channel stretches can induce local acceleration of the tidal flow with stronger ebb flow downstream of such a 'bottleneck' and stronger flood flow upstream of the 'bottleneck'. Besides, as Figure 7 is based on a single tide and Figure 6b on a spring-neap average, results do not necessarily correspond between the two types of tidal asymmetry quantification.

Adding the effect of vegetation has varying effects (i.e., comparing sc1 with sc2 and sc3), but horizontal tidal asymmetry is in all cases less flood-dominant for the scenario with the 1960s vegetation cover (i.e., sc3) than in the unvegetated scenario (i.e., sc1). This holds especially where vegetation is present, but also in the marsh channels (Figure 7). Besides, further examination of the model results indicates that the increase in total ebb volumes exceeds the increase in total flood volumes as a result of vegetation-induced flow routing, which may explain the development towards a shorter-rising tide along with a decrease in flood-dominance of the horizontal tide. If the platform elevation is increased (i.e., from sc3 to sc4), the strongly flood-dominant character of the intertidal channel diminishes (Figure 6b-c & 7). A reduction in channel size has varying effects on horizontal tidal asymmetry along the marsh channel. If the spatial patterns of ΔV_{max} are considered (Figure 7), artificial infilling of the marsh channels (i.e., comparing scenarios sc6 with sc7 and sc8) appears to enhance ebb-dominance in the outer part of the marsh channel between sections H1 and H2, whereas flood-

dominance is enhanced in the inner part (i.e., upstream of section H3) where the channel elevation is increased up to the maximum level of 2.0 m NAP (i.e., close to platform elevation). At sections H1, H2 and H3 specifically (Figure 6b-c), flood-dominance generally decreases if the channel elevation is artificially increased (i.e., sc6 to sc7 and sc8), except for the development in ΔV_{max} at the outer section H1. Finally, an increase in channel size and tidal prism at section H1 between sc5 and sc6 is accompanied by a reduction in flood-dominance, implying a decrease in flood-dominant asymmetry of the horizontal tide (Figure 6b-c).

3.4 Varying mean high water levels

Additional model runs in which geomorphological scenarios sc2 (1930s) and sc5 (1960s) are simulated with reduced tidal amplitudes (i.e., reducing the MHWL to its historical height) result in similar trends between the model scenarios and eco-geomorphological development stages. In particular, applying these reduced tidal boundary conditions leads to a 25% lower tidal prism in the marsh channels compared to the scenarios with present-day boundary conditions. Remarkably, the main indicators for tidal asymmetry ΔV_{max} (< 0.03 m/s) and R_T (< 0.03%) only differ slightly between the simulations with and without reduced tidal amplitudes. However, the proxy for residual load based on the dimensionless bed shear stress changes significantly. For the 1930s scenario (sc2), the estimated residual sediment import decreases by about 15% at sections H1 and H2, while ebb-dominance is minimized at section H3 if the tidal amplitude is reduced to that of the 1930s. For the 1960s scenario (sc5), flood-dominance at section H1 increases by ~12%, while the ebb-dominance at section H2 is minimized if the tidal amplitude is reduced to that of the 1960s. It must be stated that the simulations with reduced tidal amplitudes do not represent the exact historical situation either, as sea level rise is not incorporated and the distortion of the tidal wave along the estuary has also changed during the last decades due to geomorphological changes in the rest of the estuary (e.g. Wang et al., 2002).

4. Discussion

The aim of this study was to analyze the long-term changes in tidal asymmetry between subsequent stages of the eco-geomorphological development of a tidal marsh, starting from a relatively bare and low elevated stage to a higher elevated and vegetated tidal marsh. The present model results confirm our hypothesis of changing tidal asymmetry along with the eco-geomorphological development of tidal marshes. This implies that marsh development stage indeed influences the net transport of sediments or other materials in marsh channels. In addition, the development in tidal prism is mostly according to previous observations (Vandenbruwaene et al., 2013) and model assessments (D'Alpaos et al., 2006). That is, vegetation establishment causes flow concentration towards the marsh channels, while marsh elevation increase and hence reduced storage volume on the marsh platform lead to a decrease in tidal prism through the marsh channels. In the following paragraphs, the changes in tidal asymmetry and tidal prism during specific steps in eco-geomorphological marsh development (i.e., vegetation establishment, vertical platform growth and changes in channel geometry) are discussed in more detail.

It should be stated that based on the model results different indicators for tidal asymmetry (i.e., ΔV_{max}, R_T and the excess bed shear stress) do not always show similar trends during the different stages of marsh development. Moreover, local spatial differences in horizontal tidal asymmetry along the marsh channel appear to be large (Figure 7) compared to the long term trends or differences between the model scenarios (Figure 6b). Furthermore, the model scenarios with historical marsh bathymetries are all simulated with present-day hydrodynamic forcing, which induces relatively high tidal prisms and also affects tidal asymmetry. Finally, model validation indicates that flood-dominance of the horizontal tide is generally overestimated by the model we use (Figure 3; Table 2). Although the above deficiencies and limitations make interpretation of the model results complex, the qualitative impact of specific marsh development steps (i.e., comparing between scenarios) can still be obtained.

4.1 Effect of vegetation establishment

Our results show that tidal asymmetry initially is strongly flood-dominant on low-elevated and unvegetated tidal flats, which can be associated with a strong importing character. While previous studies showed that vegetation establishment induces channel formation or deepening associated with net sediment export hence ebb-dominance (e.g. D'Alpaos et al., 2006; French and Stoddart, 1992; Temmerman et al., 2007), the less flood-dominant

asymmetry of the horizontal tide in the present results suggests that sediment import in the marsh channels only reduces as a result of vegetation establishment. However, the net sediment import is more likely to contribute to vertical growth of the vegetated marsh platform rather than to infilling of the channel network itself as marsh vegetation enhances particle settling (e.g. Christiansen et al., 2000; de Lima et al., 2015; Mudd et al., 2010). Accordingly, higher sediment concentrations are generally moving into a marsh during flood than out of the marsh during ebb (e.g. Krone, 1987). Following the above, net sediment import through marsh channels could even be accompanied by channel erosion if sedimentation on the platform exceeds erosion in the channels. In this context, it should also be stated that flood-dominance is generally overestimated by our model. In contrast to the horizontal tide, vertical tidal asymmetry becomes more flood-dominant due to vegetation establishment (Figure 6a). This means that the lag effect vegetation has on tidal flow damps peak flood velocities more than peak ebb velocities, but it also elongates the ebb outflow. Finally, adding the effect of vegetation increases the tidal prism and moves it away from equilibrium with the cross-sectional area based on the Ω-to-P relationship for the Hondegat channel (Figure 5b). Hence, additional friction exerted by the vegetation leads to marsh scale flow concentration towards the channels, while absence of vegetation leads to more divergent sheet flow. This flow routing effect of vegetation was shown on a smaller scale in previous studies (e.g. D'Alpaos et al., 2006; Temmerman et al., 2007; Vandenbruwaene et al., 2015; Zong and Nepf, 2010).

4.2 Effect of vertical platform growth

Platform elevation increase has the largest impact on tidal hydrodynamics in marsh channels. In addition to a straightforward and expected decrease in tidal prism (e.g. D'Alpaos et al., 2006), vertical platform growth may induce contrasting effects for tidal asymmetry. It leads to a decrease in sediment demand on the marsh platform as the remaining accommodation space (i.e., space available for sedimentation; e.g. Schlager, 1993) decreases (potentially reducing flood-dominance), but a lower storage volume also implies that the channel cross-section becomes relatively large according to Ω-to-P relationships (enhancing flood-dominance). In the present study, the channel size is not exceptionally large relative to the tidal prism after the platform elevation increase (Figure 5b) and is at first accompanied by a development towards a less flood-dominant asymmetry (Figure 6 & 7). If frictional effects are considered, the impact of vertical platform growth on tidal asymmetry shows similarities with the differences in tidal asymmetry between tides with varying HWLs, for which flood-dominance

increases with the inundation height on the marsh platform (Stark et al., 2015) and hence decreases with the platform elevation. In particular, higher marsh platforms (or tides with lower platform inundation depths) exert more friction on the propagating high waters, leading to a less flood-dominant or even ebb-dominant asymmetry and vice versa. On the other hand, once the platform elevation gets sufficiently high in the tidal frame and some tides in a spring-neap cycle are confined to the channel system, the friction and storage volume provided by the marsh platform are partly lost. This is observed in the present-day scenario, in which a majority of the tides is confined within the marsh channels and the horizontal tide becomes more flood-dominant again.

4.3 Effect of changing channel geometry

Our model results show that changes in marsh channel size generally relate to variations in tidal prism through empirical relationships between tidal prism and cross-sectional areas of marsh channels (e.g. Rinaldo et al., 1999; Steel and Pye, 1997; Vandenbruwaene et al., 2015), including the Ω-to-P relationship which is established for this study (Eq. 7). In this perspective, the effect of channel infilling on tidal asymmetry may be twofold. On one hand, channel infilling reduces the cross-sectional area of the channels, which would imply that the cross-sectional area of the channel becomes relatively small based on Ω-to-P relationships, likely leading to enhanced ebb-dominance associated with channel scouring. On the other hand, marsh scale channel infilling also reduces the tidal prism itself as the water storage in the channel network decreases. The effect of changes in channel size thus depends on the position of the tidal prism and cross-sectional area relative to the Ω-to-P equilibrium curve and how important the water storage in the marsh channel network is for the total tidal prism. In addition, shallower channels may induce an increase in flood-dominant asymmetry due to stronger advective inertia and non-linear friction effects, which result in a faster propagation of the high tide than of the low tide in shallow waters and thereby enhance a flood-dominant shorter-rising asymmetry (e.g. Friedrichs and Aubrey, 1988; Speer and Aubrey, 1985). In the present model results, both decreasing and increasing flood-dominance occur as a result of reduced marsh channel size (Figure 6 & 7). For the historical scenarios in which the reduction in channel size is solely caused by channel elevation increase and in which the channel width remains constant (i.e., sc4 to sc5 at section H1, sc5 to sc6 at section H2 and H3), there is indeed an increase in flood-dominance of the horizontal tide (Figure 6b-c). Besides, the channel size decrease in these scenarios is also accompanied by an increase in platform elevation to levels around or above MHWL, causing some tides to become undermarsh and

thereby reducing the net effect of the marsh platform on tidal asymmetry. Conversely, a further decrease in channel size compared to the present-day situation reduces channel depth as well as channel width (i.e., between sc7 and sc8 at section H1 and between sc6, sc7 and sc8 at sections H2 and H3; Figure 4d), and induces a development towards a more ebb-dominant asymmetry (Figure 6b-c & 7). In this case, hydro-morphodynamic feedbacks may enlarge the channel size to its equilibrium cross-section based on the above mentioned Ω-to-P relationships after the channel size is reduced. However, along the innermost part of the channel (i.e., upstream of section H3), flood-dominance increases again after the channel elevation is almost increased up to platform elevation (Figure 7). This suggests that the hydro-morphodynamic feedback mechanism that keeps the channel open does not persist if the channel elevation increases too much (i.e. in this case for channel elevations > 2.0 m NAP) or the tidal prism becomes too small. Based on this, we hypothesize that there are two morphological states to which intertidal marsh channels may develop if they are brought out of equilibrium by a reduction in channel size or tidal prism; (1) a state in which velocities remain high enough to erode the channel bed and enlarge the channel depth according to typical Ω-to-P relationships and (2) a state in which velocities are too low to erode the channel bed leading to a complete infilling and siltation of the marsh channel. This reasoning is similar to the response of tidal inlets to changes in cross-sectional area or tidal prism and flow velocities, typically examined by closure curves such as the Escoffier (1940) curve (e.g. De Swart and Zimmerman, 2009).

4.4 Concluding remarks

In conclusion, the present study shows how the eco-geomorphological development stage of marshes influences tidal asymmetry in marsh channels and hence determines the net import or export of sediments or other materials and whether marsh systems act as a sink or source. Our results may assist scientists and managers of tidal marshes in understanding the interactions between tidal hydrodynamics and the geomorphological development of marshes and marsh channels in particular. On the other hand, areas where sea level rise or sediment depletion cause drowning and die-off of tidal wetlands (e.g. Kirwan and Megonigal, 2013; Kirwan et al., 2016) could also benefit from this study, especially as the effect of higher tidal amplitudes and mean high water levels was indirectly assessed in the historical scenarios. Furthermore, the results could open a route for research on the stability of marsh channels as a result of changes in tidal hydrodynamics or sediment supply and whether channel siltation may occur or not. Finally, the present study is of interest to scientists or estuarine managers studying

marsh ecology as long-term variations in tidal prism or asymmetry also affect the ecological functioning of marshes through changes in the exchange of water, sediments and other particulate matter between marshes and adjacent water bodies (e.g. Fagherazzi et al., 2013, 2012). This time-varying impact on ecological functioning is also reflected in the ecosystem services provided by intertidal areas during different stages of marsh development (Boerema et al., 2016).

Acknowledgements

We would like to thank the Port of Antwerp for funding this research, CalcUA for their support and for the usage of their HPC environment and C. Schwarz, G. Schramkowski, R. Brouwer, A. Nnafie and B. Borsje for their feedback and useful suggestions.

References

Allen, J.R.L., 2000. Morphodynamics of Holocene salt marshes: A review sketch from the Atlantic and Southern North Sea coasts of Europe. Quat. Sci. Rev. 19, 1155–1231. doi:10.1016/S0277-3791(99)00034-7

Aubrey, D.G., Speer, P.E., 1985. A Study of Non-linear Tidal Propagation in shallow inlet / estuarine systems Part I : Observations. Estuar. Coast. Shelf Sci. 21, 185–205.

Baptist, M.J., Babovic, V., Rodríguez Uthurburu, J., Keijzer, M., Uittenbogaard, R.E., Mynett, A., Verwey, A., 2007. On inducing equations for vegetation resistance. J. Hydraul. Res. 45, 435–450.

Barbier, E.B., Georgiou, I.Y., Enchelmeyer, B., Reed, D.J., 2013. The value of wetlands in protecting Southeast Louisiana from hurricane storm surges. PLoS One 8, e58715. doi:10.1371/journal.pone.0058715

Boerema, A., Geerts, L., Oosterlee, L., Temmerman, S., Meire, P., 2016. Ecosystem service delivery in restoration projects: The effect of ecological succession on the benefits of tidal marsh restoration. Ecol. Soc. 21. doi:10.5751/ES-08372-210210

Boon, J.D.I., 1975. Tidal discharge asymmetry in a salt marsh drainage system. Limnol. Oceanogr. 20, 71–80. doi:10.4319/lo.1975.20.1.0071

Bouma, T.J., Temmerman, S., van Duren, L.A., Martini, E., Vandenbruwaene, W., Callaghan, D.P., Balke, T., Biermans, G., Klaassen, P.C., van Steeg, P., Dekker, F., van de Koppel, J., de Vries, M.B., Herman, P.M.J., 2013. Organism traits determine the strength of scale-dependent bio-geomorphic feedbacks: A flume study on three intertidal plant species. Geomorphology 180-181, 57–65. doi:10.1016/j.geomorph.2012.09.005

Chollet, J.P., Cunge, J.A., 1979. New interpretation of some head loss-flow velocity relationships for deformable movable beds. J. Hydraul. Res. 17, 1–13. doi:10.1080/00221687909499596

Christiansen, T., Wiberg, P.L., Milligan, T.G., 2000. Flow and Sediment Transport on a Tidal Salt Marsh Surface. Estuar. Coast. Shelf Sci. 50, 315–331. doi:10.1006/ecss.2000.0548

D'Alpaos, A., Lanzoni, S., Marani, M., Fagherazzi, S., Rinaldo, A., 2005. Tidal network ontogeny: Channel initiation and early development. J. Geophys. Res. Earth Surf. 110,

1–14. doi:10.1029/2004JF000182

D'Alpaos, A., Lanzoni, S., Marani, M., Rinaldo, A., 2009. On the O'Brien–Jarrett–Marchi law. Rend. Lincei 20, 225–236. doi:10.1007/s12210-009-0052-x

D'Alpaos, A., Lanzoni, S., Marani, M., Rinaldo, A., 2007. Landscape evolution in tidal embayments: Modeling the interplay of erosion, sedimentation, and vegetation dynamics. J. Geophys. Res. Earth Surf. 112, 1–17. doi:10.1029/2006JF000537

D'Alpaos, A., Lanzoni, S., Mudd, S.M., Fagherazzi, S., 2006. Modeling the influence of hydroperiod and vegetation on the cross-sectional formation of tidal channels. Estuar. Coast. Shelf Sci. 69, 311–324. doi:10.1016/j.ecss.2006.05.002

De Lima, P.H.S., Janzen, J.G., Nepf, H.M., 2015. Flow patterns around two neighboring patches of emergent vegetation and possible implications for deposition and vegetation growth. Environ. Fluid Mech. 881–898. doi:10.1007/s10652-015-9395-2

De Swart, H.E., Zimmerman, J.T.F., 2009. Morphodynamics of Tidal Inlet Systems. Annu. Rev. Fluid Mech. 41, 203–229. doi:10.1146/annurev.fluid.010908.165159

Dronkers, J., 1986. Tidal asymmetry and estuarine morphology. Netherlands J. Sea Res. 20, 117–131. doi:10.1016/0077-7579(86)90036-0

Escoffier, F.F., 1940. The stability of tidal inlets. Shore and Beach 8, 114–115.

Fagherazzi, S., Kirwan, M.L., Mudd, S.M., Guntenspergen, G.R., Temmerman, S., Rybczyk, J.M., Reyes, E., Craft, C., Clough, J., 2012. Numerical models of salt marsh evolution: Ecological, geormorphic, and climatic factors 1–28. doi:10.1029/2011RG000359.1.INTRODUCTION

Fagherazzi, S., Wiberg, P.L., Temmerman, S., Struyf, E., Zhao, Y., Raymond, P.A., 2013. Fluxes of water, sediments, and biogeochemical compounds in salt marshes. Ecol. Process. 2, 3. doi:10.1186/2192-1709-2-3

French, J.R., Stoddart, D.R., 1992. Hydrodynamics of Salt Marsh Creek Systems: Implications for Marsh Morphological Development and Material Exchange. Earth Surf. Process. Landforms 17, 235–252.

French, P.W., 2006. Managed realignment - The developing story of a comparatively new approach to soft engineering. Estuar. Coast. Shelf Sci. 67, 409–423. doi:10.1016/j.ecss.2005.11.035

Friedrichs, C.T., Aubrey, D.G., 1988. Non-linear Tidal Distortion in Shallow Well-Mixed Estuaries: a Synthesis. Estuar. Coast. Shelf Sci. 27, 521–545. doi:10.1016/0272-7714(90)90054-U

Friedrichs, C.T., Perry, J.E., 2001. Tidal salt marsh morphodynamics: A Synthesis. J. Coast. Res. 27, 7–37.

Ganju, N.K., Kirwan, M.L., Dickhudt, P.J., Guntenspergen, G.R., Cahoon, D.R., Kroeger, K.D., 2015. Sediment transport-based metrics of wetland stability. Geophys. Res. Lett. 42, 7992–8000. doi:10.1002/2015GL065980

Ganju, N.K., Nidzieko, N.J., Kirwan, M.L., 2013. Inferring tidal wetland stability from channel sediment fluxes: Observations and a conceptual model. J. Geophys. Res. Earth Surf. 118, 2045–2058. doi:10.1002/jgrf.20143

Gedan, K.B., Kirwan, M.L., Wolanski, E., Barbier, E.B., Silliman, B.R., 2010. The present and future role of coastal wetland vegetation in protecting shorelines: Answering recent

challenges to the paradigm. Clim. Change 106, 7–29. doi:10.1007/s10584-010-0003-7

Green, M.O., Hancock, N.J., 2012. Sediment transport through a tidal creek. Estuar. Coast. Shelf Sci. 109, 116–132. doi:10.1016/j.ecss.2012.05.030

Hampel, H., Catrijsse, A., Vincx, M., 2003. Morphometric variation among sardine (Sardina pilchardus) populations from the northeastern Atlantic and the western Mediterranean. ICES J. Mar. Sci. J. du … 60, 278–289. doi:10.1016/S1054

Hervouet, J.-M., 2007. Hydrodynamics of Free Surface Flows: Modelling with the finite element method. doi:10.1002/9780470319628

Huijs, S., 1995. Geomorfologische ontwikkeling van het intergetijdegebied in de Westerschelde 1935-1989. Middelburg, The Netherlands.

Jarrett, J.T., 1976. Tidal Prism - Inlet Area Relationships. Vicksburg, MS, U.S.

Jongepier, I., Wang, C., Missiaen, T., Soens, T., Temmerman, S., 2015. Intertidal landscape response time to dike breaching and stepwise re-embankment: A combined historical and geomorphological study. Geomorphology 236, 64–78. doi:10.1016/j.geomorph.2015.02.012

Kirwan, M.L., Guntenspergen, G.R., D'Alpaos, A., Morris, J.T., Mudd, S.M., Temmerman, S., 2010. Limits on the adaptability of coastal marshes to rising sea level. Geophys. Res. Lett. 37, n/a–n/a. doi:10.1029/2010GL045489

Kirwan, M.L., Megonigal, J.P., 2013. Tidal wetland stability in the face of human impacts and sea-level rise. Nature 504, 53–60. doi:10.1038/nature12856

Kirwan, M.L., Murray, a B., 2007. A coupled geomorphic and ecological model of tidal marsh evolution. Proc. Natl. Acad. Sci. U. S. A. 104, 6118–6122. doi:10.1073/pnas.0700958104

Kirwan, M.L., Temmerman, S., Skeehan, E.E., Guntenspergen, G.R., Fagherazzi, S., 2016. Overestimation of marsh vulnerability to sea level rise. Nat. Clim. Chang. 6, 253–260. doi:10.1038/nclimate2909

Krone, R.B., 1987. A method for simulating historic marsh elevations, in: Krause, N.C. (Ed.), Coastal Sediments '87. American Society of Civil Engineers, New York, NY, pp. 316–323.

McLeod, E., Chmura, G.L., Bouillon, S., Salm, R., Björk, M., Duarte, C.M., Lovelock, C.E., Schlesinger, W.H., Silliman, B.R., 2011. A blueprint for blue carbon: Toward an improved understanding of the role of vegetated coastal habitats in sequestering CO2. Front. Ecol. Environ. 9, 552–560. doi:10.1890/110004

Mitsch, W.J., Bernal, B., Nahlik, A.M., Mander, Ü., Zhang, L., Anderson, C.J., Jørgensen, S.E., Brix, H., 2013. Wetlands, carbon, and climate change. Landsc. Ecol. 28, 583–597. doi:10.1007/s10980-012-9758-8

Mitsch, W.J., Zhang, L., Stefanik, K.C., Nahlik, A.M., Anderson, C.J., Bernal, B., Hernandez, M., Song, K., 2012. Creating Wetlands: Primary Succession, Water Quality Changes, and Self-Design over 15 Years. Bioscience 62, 237–250. doi:10.1525/bio.2012.62.3.5

Mudd, S.M., D'Alpaos, A., Morris, J.T., 2010. How does vegetation affect sedimentation on tidal marshes? Investigating particle capture and hydrodynamic controls on biologically mediated sedimentation. J. Geophys. Res. 115, F03029. doi:10.1029/2009JF001566

O'Brien, M.P., 1969. Equilibrium flow areas of tidal inlets on sandy coasts, in: Proceedings of

the American Society of Civil Engineers. Journal of the Waterways and Harbors Division. pp. 43–52–. doi:10.9753/icce.v10.25p

O'Brien, M.P., 1931. Estuary and tidal prisms related to entrance areas. Civ. Eng. 1, 738–739.

Ouyang, X., Lee, S.Y., 2014. Updated estimates of carbon accumulation rates in costal marsh sediments. Biogeosciences Discuss. 11, 5057–5071. doi:10.5194/bgd-10-19155-2013

Parker, B.B., 1984. Frictional effects on the tidal dynamics of a shallow estuary, Ph.D. thesis. John Hopkins University, Baltimore, Md., U.S.A.

Pethick, J.S., 1980. Velocity surges and asymmetry in tidal channels. Estuar. Coast. Mar. Sci. 11, 331–345. doi:10.1016/S0302-3524(80)80087-9

Reed, D.J., 2002. Sea-level rise and coastal marsh sustainability: Geological and ecological factors in the Mississippi delta plain. Geomorphology 48, 233–243. doi:10.1016/S0169-555X(02)00183-6

Rinaldo, A., Fagherazzi, S., Lanzoni, S., Marani, M., Dietrich, W.E., 1999. Tidal networks: 3. Landscape-forming discharges and studies in empirical geomorphic relationships. Water Resour. Res. 35, 3919–3929.

Schlager, W., 1993. Accommodation and supply a dual control on stratigraphic sequences. Sediment. Geol. 86, 111–136. doi:10.1016/0037-0738(93)90136-S

Smolders, S., Ides, S., Plancke, Y., Meire, P., Temmerman, S., 2012. Calibrating Discharges in a 2D Hydrodynamic Model of the Scheldt Estuary : Which Parameters Can Be Used and What Is Their Sensitivity ?, in: Proceedings of 10th International Conference on Hydroinformatics, HIC 2012, Hamburg, Germany. p. 8.

Smolders, S., Plancke, Y., Ides, S., Meire, P., Temmerman, S., 2015. Role of intertidal wetlands for tidal and storm tide attenuation along a confined estuary: A model study. Nat. Hazards Earth Syst. Sci. 15, 1659–1675. doi:10.5194/nhess-15-1659-2015

Spalding, M.D., McIvor, A.L., Beck, M.W., Koch, E.W., Möller, I., Reed, D.J., Rubinoff, P., Spencer, T., Tolhurst, T.J., Wamsley, T. V., van Wesenbeeck, B.K., Wolanski, E., Woodroffe, C.D., 2014. Coastal Ecosystems: A Critical Element of Risk Reduction. Conserv. Lett. 7, 293–301. doi:10.1111/conl.12074

Speer, P.E., Aubrey, D.G., 1985. A study of non-linear tidal propagation in shallow inlet/estuarine systems Part II: Theory. Estuar. Coast. Shelf Sci. 21, 207–224. doi:10.1016/0272-7714(85)90097-6

Stark, J., Plancke, Y., Ides, S., Meire, P., Temmerman, S., 2016. Coastal flood protection by a combined nature-based and engineering approach: Modeling the effects of marsh geometry and surrounding dikes. Estuar. Coast. Shelf Sci. 175, 34–45. doi:10.1016/j.ecss.2016.03.027

Stark, J., Van Oyen, T., Meire, P., Temmerman, S., 2015. Observations of tidal and storm surge attenuation in a large tidal marsh. Limnol. Oceanogr. 60, 1371–1381. doi:10.1002/lno.10104

Steel, T.J., Pye, K., 1997. The development of saltmarsh tidal creek networks: evidence from the UK., in: Proceedings of the Canadian Coastal Conference, 22-25 May 1997. pp. 267–280.

Stefanon, L., Carniello, L., D'Alpaos, A., Lanzoni, S., 2010. Experimental analysis of tidal network growth and development. Cont. Shelf Res. 30, 950–962. doi:10.1016/j.csr.2009.08.018

Stive, M.J.F., Ji, L., Brouwer, R.L., van de Kreeke, J., Ranasinghe, R., 2010. Empirical relationship between inlet cross-sectional area and tidal prism: a re-evaluation, in: Proceedings of the 32nd International Conference on Coastal Engineering, ICCE 2010, Shanghai, China, 30-5 July 2010, 1-10.

Struyf, E., Van Damme, S., Gribsholt, B., Meire, P., 2005. Freshwater marshes as dissolved silica recyclers in an estuarine environment (Schelde estuary, Belgium). Hydrobiologia 540, 69–77. doi:10.1007/s10750-004-7104-0

Temmerman, S., Bouma, T.J., Van de Koppel, J., Van der Wal, D., De Vries, M.B., Herman, P.M.J., 2007. Vegetation causes channel erosion in a tidal landscape. Geology 35, 631. doi:10.1130/G23502A.1

Temmerman, S., Govers, G., Meire, P., Wartel, S., 2003. Modelling long-term tidal marsh growth under changing tidal conditions and suspended sediment concentrations, Scheldt estuary, Belgium. Mar. Geol. 193, 151–169. doi:10.1016/S0025-3227(02)00642-4

Temmerman, S., Govers, G., Wartel, S., Meire, P., 2004. Modelling estuarine variations in tidal marsh sedimentation: Response to changing sea level and suspended sediment concentrations. Mar. Geol. 212, 1–19. doi:10.1016/j.margeo.2004.10.021

Temmerman, S., Kirwan, M.L., 2015. Building land with a rising sea. Science (80-.). 349, 588–589. doi:10.1126/science.aac8312

Temmerman, S., Meire, P., Bouma, T.J., Herman, P.M.J., Ysebaert, T., De Vriend, H.J., 2013. Ecosystem-based coastal defence in the face of global change. Nature 504, 79–83. doi:10.1038/nature12859

Temmerman, S., Moonen, P., Schoelynck, J., Govers, G., Bouma, T.J., 2012. Impact of vegetation die-off on spatial flow patterns over a tidal marsh. Geophys. Res. Lett. 39. doi:10.1029/2011GL050502

Tolman, M.E., Pranger, D.P., 2012. Toelichting bij de Vegetatiekartering Westerschelde 2010.

Van de Kreeke, J., Robaczewska, K., 1993. Tide-induced residual transport of coarse sediment; Application to the EMS estuary. Netherlands J. Sea Res. 31, 209–220. doi:10.1016/0077-7579(93)90022-K

Van Rijn, L.C., 2007a. Unified View of Sediment Transport by Currents and Waves. I: Initiation of Motion, Bed Roughness, and Bed-Load. J. Hydraul. Eng. 133, 649–667. doi:van Rijn, L.C., 2007. Unified View of Sediment Transport by Currents and Waves. I: Initiation of Motion, Bed Roughness, and Bed-Load. J. Hydraul. Eng. 133, 649–667. doi:10.1061/(ASCE)0733-9429(2007)133:6(649)

Van Rijn, L.C., 2007b. Unified View of Sediment Transport by Currents and Waves. II: Suspended Transport. J. Hydraul. Eng. 133, 668–389. doi: 10.1061/(ASCE)0733-9429(2007)133:6(668)

Van Rijn, L.C., 1993. Principles of Sediment Transport in Rivers, Estuaries and Coastal Seas. Aqua Publications, Amsterdam.

Vandenbruwaene, W., Bouma, T.J., Meire, P., Temmerman, S., 2013. Bio-geomorphic effects on tidal channel evolution: Impact of vegetation establishment and tidal prism change. Earth Surf. Process. Landforms 38, 122–132. doi:10.1002/esp.3265

Vandenbruwaene, W., Schwarz, C., Bouma, T.J., Meire, P., Temmerman, S., 2015. Landscape-scale flow patterns over a vegetated tidal marsh and an unvegetated tidal flat:

implications for the landform properties of the intertidal floodplain. Geomorphology 231, 40–52. doi:10.1016/j.geomorph.2014.11.020

Vanlierde, E., Vereecken, H., Plancke, Y., Taverniers, E., Mostaert, F., 2013. MONEOS - jaarboek monitoring WL 2012: Factual data rapportage van monitoring hydrodynamiek en fysische parameters zoals gemeten door WL in het Zeescheldebekken in 2012. Versie 2.0. WL Rapporten, 12_070. Antwerpen.

Wang, C., Temmerman, S., 2013. Does biogeomorphic feedback lead to abrupt shifts between alternative landscape states?: An empirical study on intertidal fl ats and marshes. J. Geophys. Res. 118, 229–240. doi:10.1029/2012JF002474

Wang, Z., Jeuken, C., De Vriend, H., 1999. Tidal asymmetry and residual sediment transport in estuaries. A literature study and applications to the Western Scheldt, Z2749.

Wang, Z.B., Jeuken, M.C.J.L., Gerritsen, H., De Vriend, H.J., Kornman, B.A., 2002. Morphology and asymmetry of the vertical tide in the Westerschelde estuary. Cont. Shelf Res. 22, 2599–2609. doi:10.1016/S0278-4343(02)00134-6

Ysebaert, T., Herman, P.M.J., 2002. Spatial and temporal variation in benthic macrofauna and relationships with environmental variables in an estuarine, intertidal soft-sediment environment. Mar. Ecol. Prog. Ser. 244, 105–124. doi:10.3354/meps244105

Zong, L., Nepf, H., 2010. Flow and deposition in and around a finite patch of vegetation. Geomorphology 116, 363–372. doi:10.1016/j.geomorph.2009.11.020

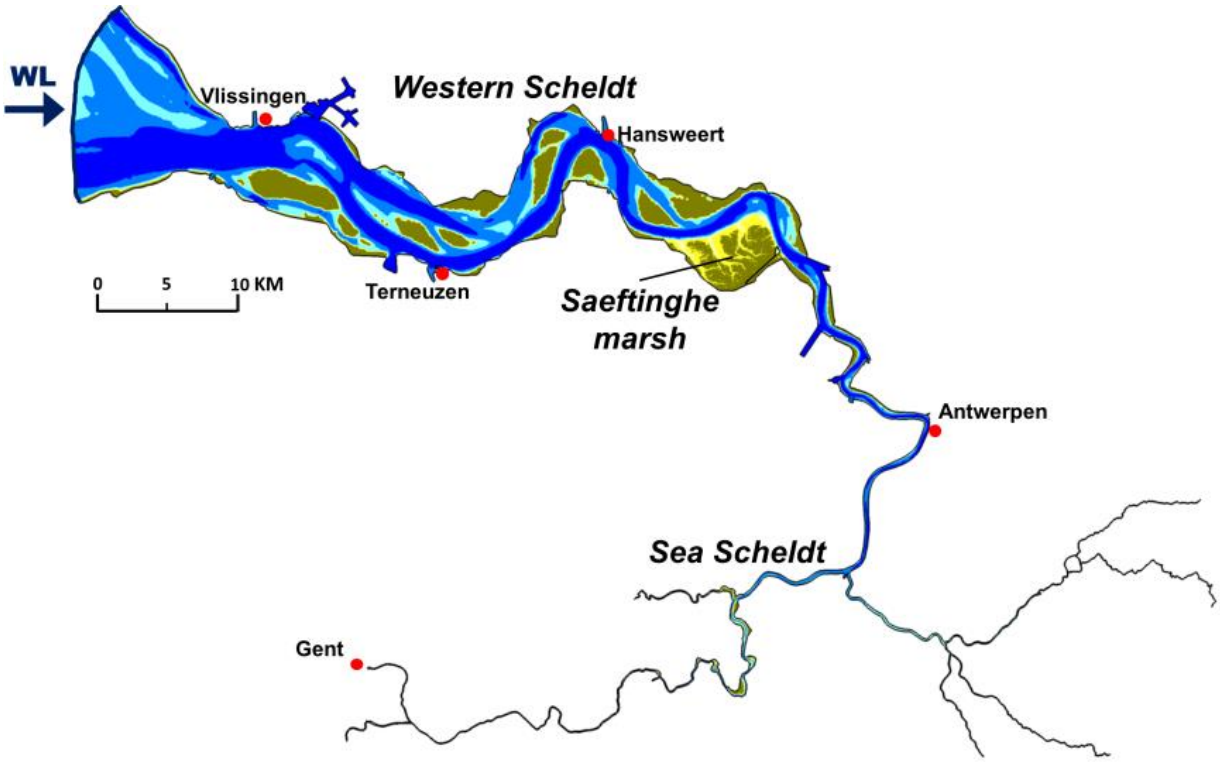

Figure 1: Scheldt Estuary and its intertidal areas (in brown and yellow), including the Saeftinghe marsh.

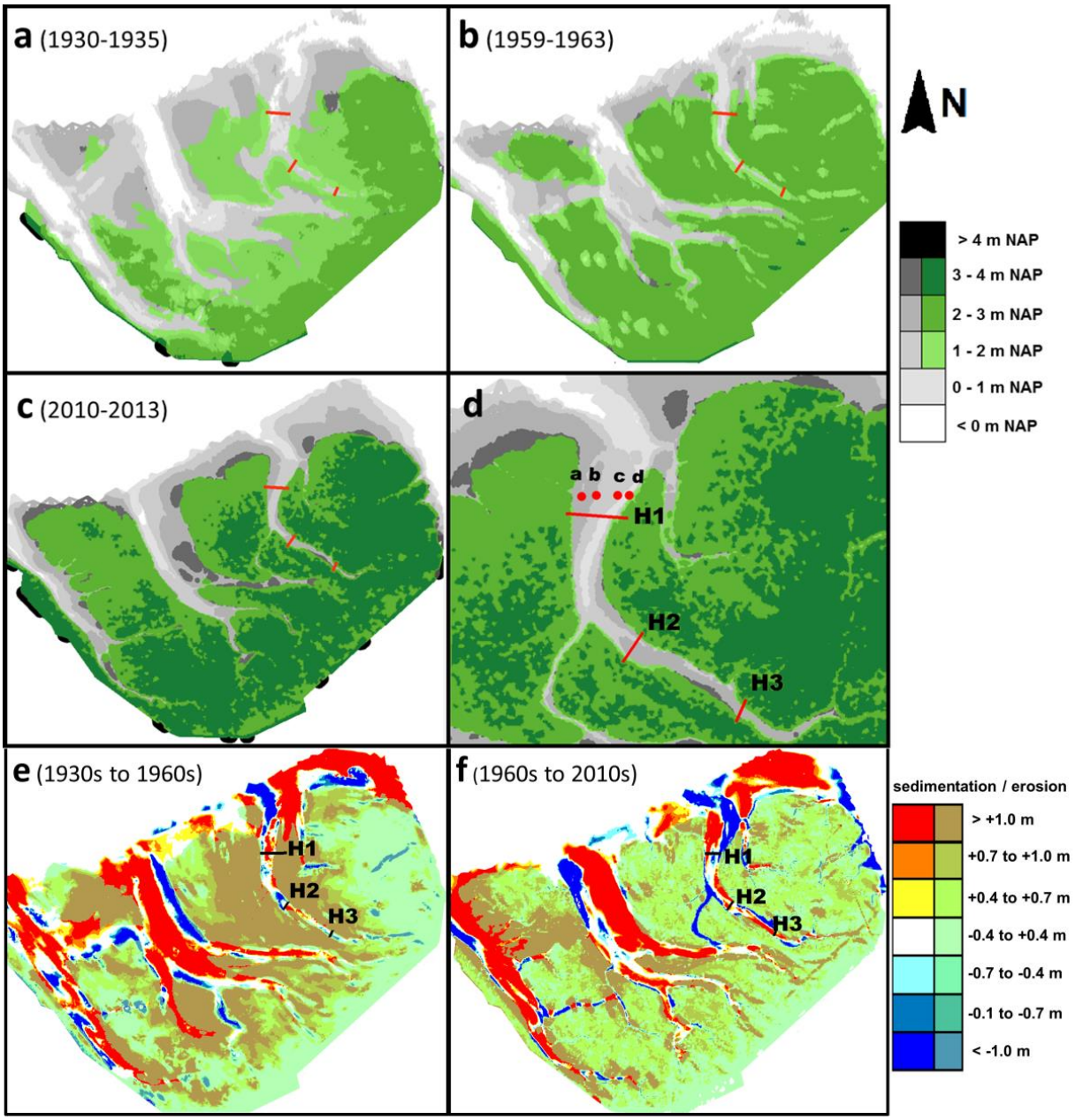

Figure 2: Map of the Saeftinghe marsh, shown with the bathymetry and vegetation cover of a) 1930-1935, b) 1959-1963 and c) 2010-2013; d) the studied marsh channel with the locations of the velocity measurements and the sections where tidal hydrodynamics are assesed indicated in red and the historical elevation changes in the Saeftinghe marsh between (e) the 1930s and 1960s and (f) the 1960s and 2010s.

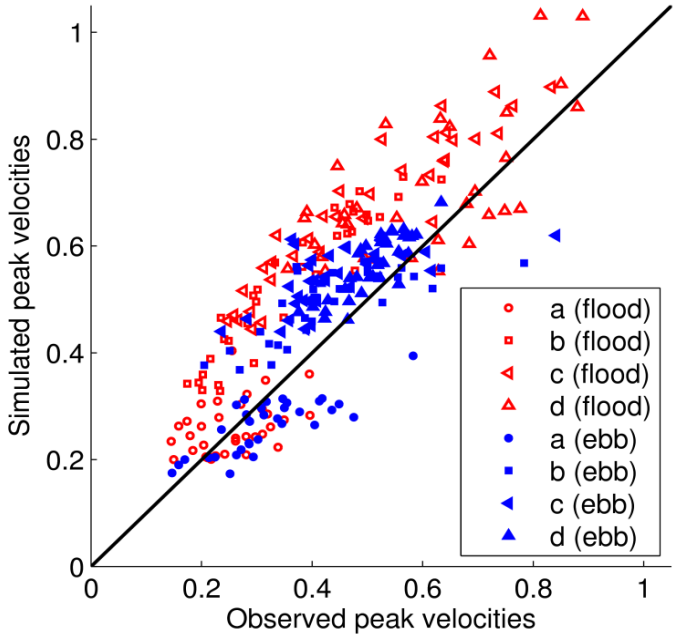

Figure 3: Simulated against observed peak flow velocities during flood (red markers) and ebb (blue markers) at velocity measurement locations a, b, c and d.

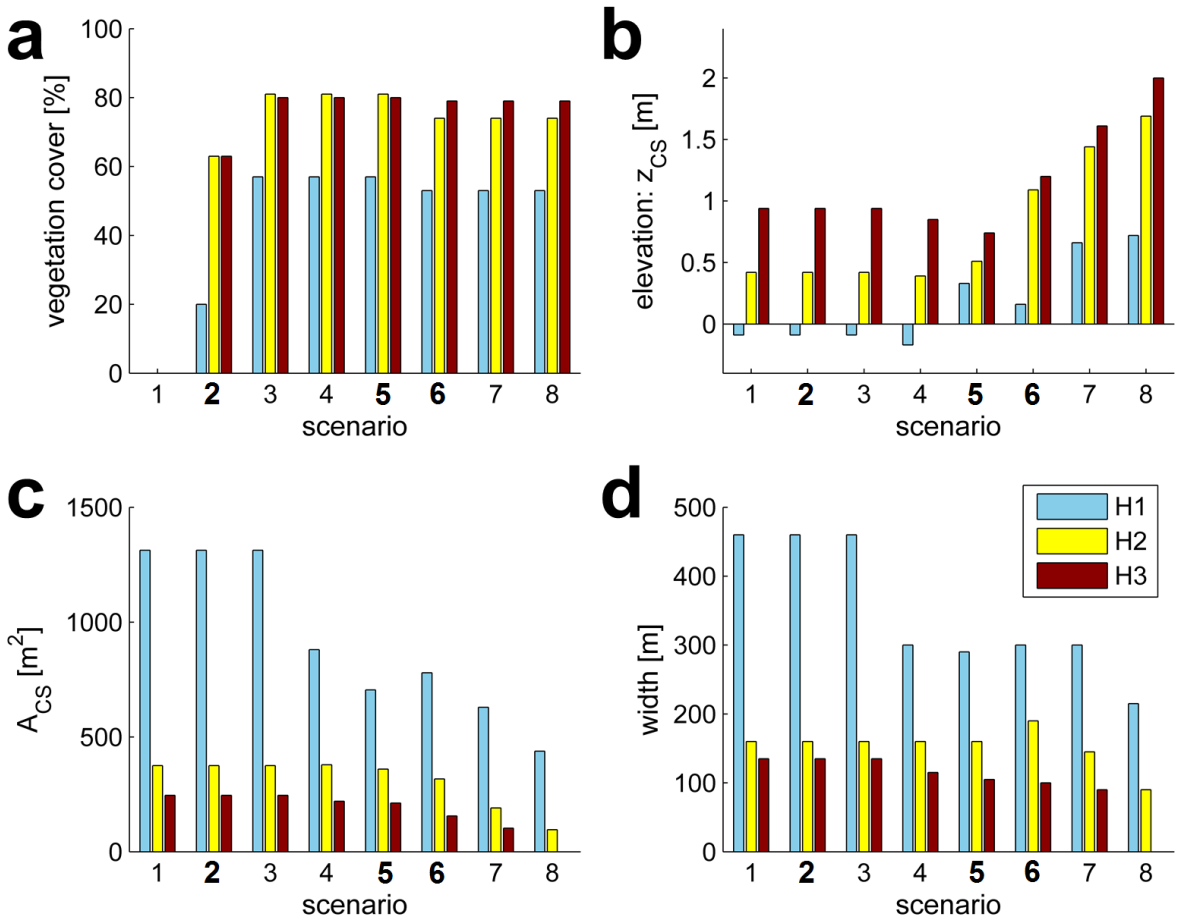

Figure 4: Geomorphological development of the Hondegat channel for the modelled scenarios at cross sections H1, H2 and H3 (see Figure 1 for locations) showing (a) the vegetation cover for a 500 m wide buffer zone around the channel cross-section, (b) the mean elevation of the cross-section, (c) the cross-sectional area below MHWL and (d) the channel width. The historical scenarios are indicated in bold.

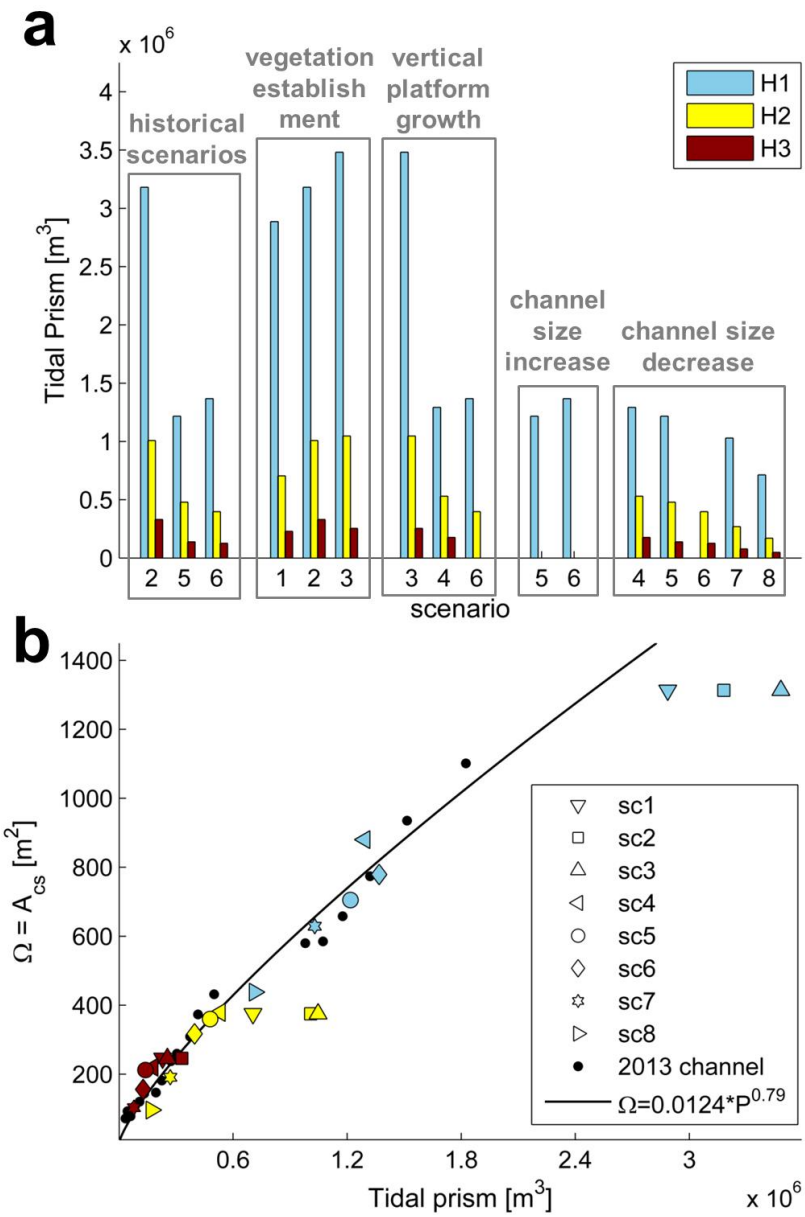

Figure 5: (a) Simulated mean flood tidal prism through cross-sections H1, H2 and H3 and (b) tidal prism plotted against the cross-sectional areas of section H1 (blue), H2 (yellow) and H3 (dark red) for scenarios sc1-sc8. The plotted power law relationship (Eq. 7) is based on the simulated tidal prism through multiple cross-sections of the marsh channel in the 2013 bathymetry (black dots).

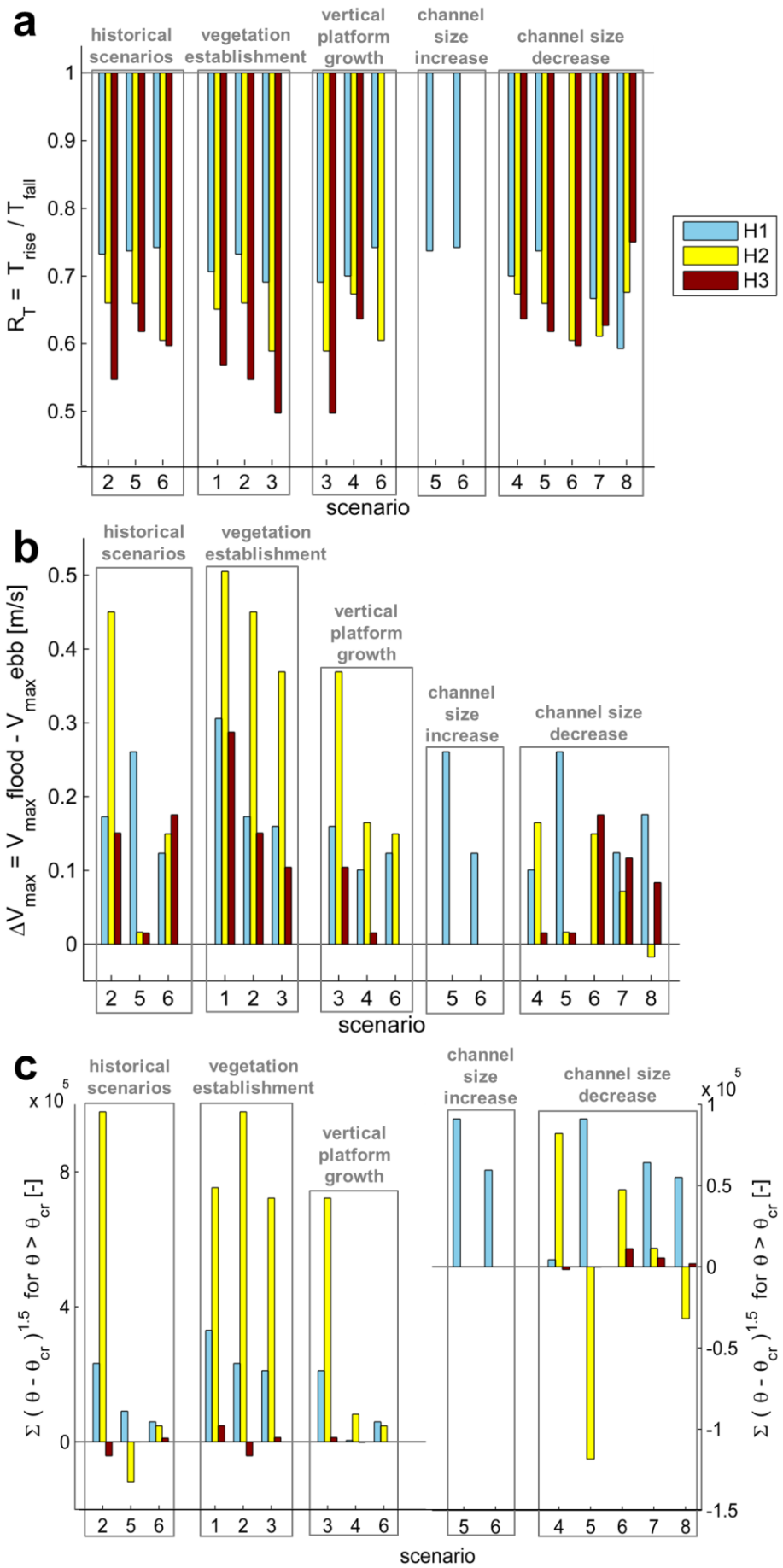

Figure 6: Modelled tidal asymmetry at locations H1, H2 and H3 for scenarios sc1-sc8 based on (a) the ratio between flood and ebb periods R_T, (b) the difference between cross-sectional averaged peak flood and ebb peak velocities $\Delta Vmax$ and (c) a proxy for residual sediment transport based on the excess dimensionless bed shear stress (see: Eq. 3-6). Note the different scaling of the vertical axes on the left and right side of Figure 6c, in which positive values denote a flood-dominant asymmetry and negative values an ebb-dominant asymmetry.

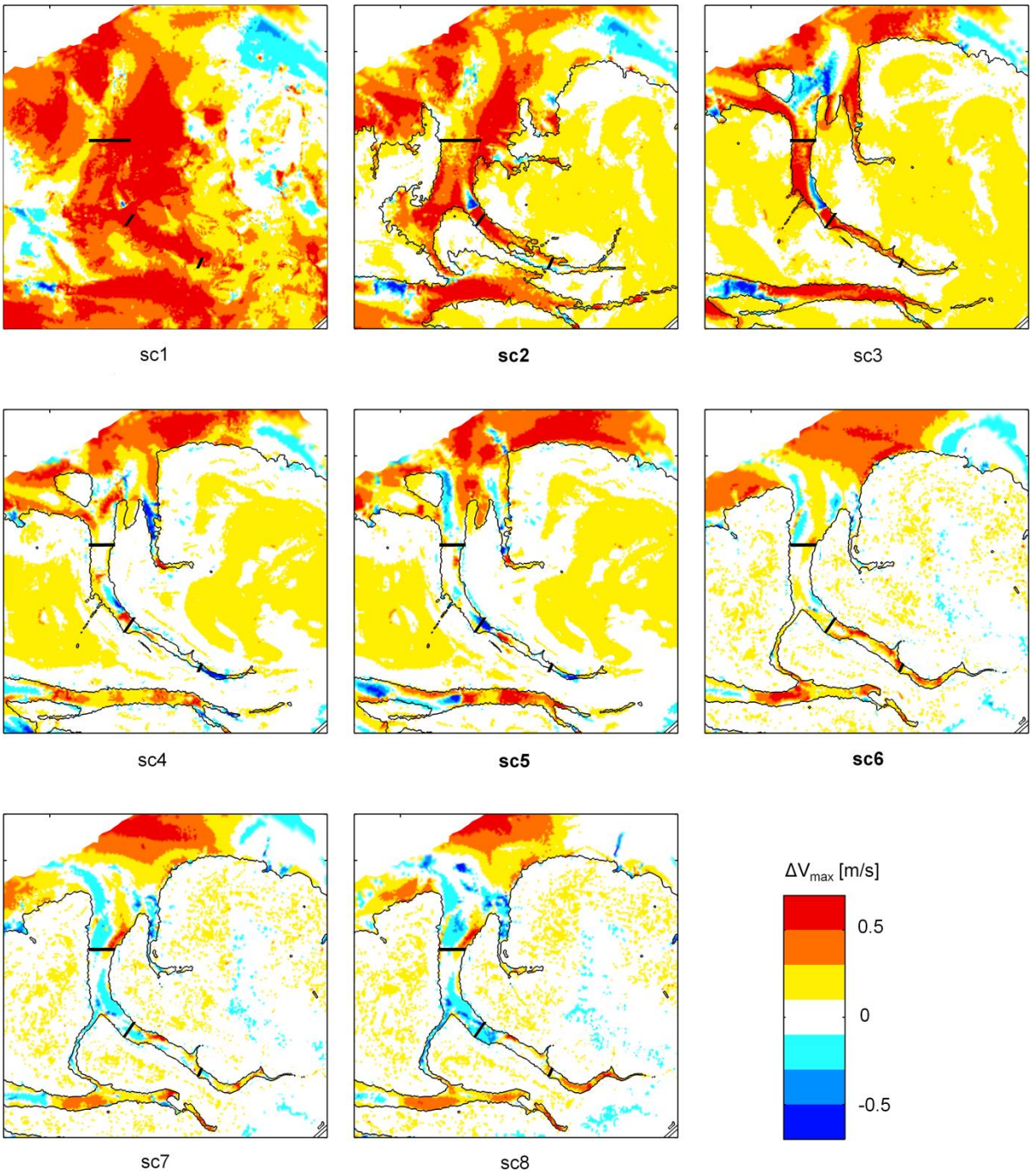

Figure 7: Difference between peak flood velocities and peak ebb velocities (ΔVmax) along the Hondegat channel and its surrounding platform for a single spring tide with a high water level of +3.15 m NAP for scenarios sc1-sc8. The historical scenarios are indicated in bold. The contour lines represent the border between the vegetated and non-vegetated parts of the marsh for each scenario.